

# An Allelic Mutant Series of *ATM3* Reveals Its Key Role in the Biogenesis of Cytosolic Iron-Sulfur Proteins in *Arabidopsis*<sup>1[C][W][OA]</sup>

Delphine G. Bernard, Youfa Cheng, Yunde Zhao, and Janneke Balk\*

Department of Plant Sciences, University of Cambridge, Cambridge CB2 3EA, United Kingdom (D.G.B., J.B.); and Section of Cell and Developmental Biology, University of California San Diego, La Jolla, California 92093-0116 (Y.C., Y.Z.)

The ATP-binding cassette transporters of mitochondria (ATMs) are highly conserved proteins, but their function in plants is poorly defined. *Arabidopsis* (*Arabidopsis thaliana*) has three *ATM* genes, namely *ATM1*, *ATM2*, and *ATM3*. Using a collection of insertional mutants, we show that only *ATM3* has an important function for plant growth. Additional *atm3* alleles were identified among sirtinol-resistant lines, correlating with decreased activities of aldehyde oxidases, cytosolic enzymes that convert sirtinol into an auxin analog, and depend on iron-sulfur (Fe-S) and molybdenum cofactor (Moco) as prosthetic groups. In the sirtinol-resistant *atm3-3* allele, the highly conserved arginine-612 is replaced by a lysine residue, the negative effect of which could be mimicked in the yeast *Atm1p* ortholog. *Arabidopsis atm3* mutants displayed defects in root growth, chlorophyll content, and seedling establishment. Analyses of selected metal enzymes showed that the activity of cytosolic aconitase (Fe-S) was strongly decreased across the range of *atm3* alleles, whereas mitochondrial and plastid Fe-S enzymes were unaffected. Nitrate reductase activity (Moco, heme) was decreased by 50% in the strong *atm3* alleles, but catalase activity (heme) was similar to that of the wild type. Strikingly, in contrast to mutants in the yeast and mammalian orthologs, *Arabidopsis atm3* mutants did not display a dramatic iron homeostasis defect and did not accumulate iron in mitochondria. Our data suggest that *Arabidopsis ATM3* may transport (1) at least two distinct compounds or (2) a single compound required for both Fe-S and Moco assembly machineries in the cytosol, but not iron.

Plant cells contain more than 50 iron-sulfur (Fe-S) enzymes that carry out important redox and catalytic functions in many aspects of metabolism (Imsande, 1999; Balk and Lobréaux, 2005). The assembly of Fe-S cofactors is mediated by dedicated machinery of ancient evolutionary origin. In plants, mitochondria harbor homologs of the bacterial ISC (for iron sulfur cluster) proteins, while plastids have inherited the sulfur mobilization machinery from their cyanobacterial ancestor (Balk and Lobréaux, 2005; Kessler and Papenbrock, 2005; Pilon et al., 2006). Plant cytosol contains homologs of the cytosolic Fe-S assembly proteins that have recently been identified in yeast (Lill and Mühlenhoff, 2008), including the scaffold

protein AtNBP35 (Bych et al., 2008; Kohbushi et al., 2009) and the hydrogenase-like AtNAR1 (Cavazza et al., 2008). It is thought that cytosolic Fe-S cluster assembly is dependent on at least one of the organelles, because the Cys desulfurases that generate sulfur for Fe-S clusters, CpNifS and NFS1, are strictly localized in the plastids and mitochondria, respectively (Kushnir et al., 2001; Frazzon et al., 2007; Van Hoewyk et al., 2007).

In yeast, cytosolic and nuclear Fe-S cluster assembly depends on the mitochondrial ISC pathway and on the ATP-binding cassette (ABC) transporter of the mitochondria, *Atm1p* (Kispal et al., 1999). *Atm1p* is classified as a “half-transporter” that functions as a homodimer and is localized in the mitochondrial inner membrane with the ATPase domains at the matrix side (Leighton and Schatz, 1995). The orientation indicates that the direction of transport is from the mitochondrial matrix to the intermembrane space and cytosol. In accordance, mutations of yeast *ATM1* cause a defect in cytosolic/nuclear Fe-S cluster assembly but not in mitochondrial Fe-S cluster assembly (Kispal et al., 1999). The substrates of *Atm1p*, however, or of its functional orthologs in other eukaryotes have not been identified thus far.

Yeast *atm1* mutations also disrupt iron homeostasis: iron uptake transporters are constitutively expressed independent of the iron concentration, and iron accumulates 10- to 30-fold in the mitochondria (Kispal

<sup>1</sup> This work was supported by a University Research Fellowship from the Royal Society to J.B., by the Brooks Fund and a Marie Curie Intra-European Fellowship to D.G.B., and by the National Institutes of Health (grant no. R01GM68631 to Y.Z.).

\* Corresponding author; e-mail [jb511@cam.ac.uk](mailto:jb511@cam.ac.uk).

The author responsible for distribution of materials integral to the findings presented in this article in accordance with the policy described in the Instructions for Authors ([www.plantphysiol.org](http://www.plantphysiol.org)) is: Janneke Balk ([jb511@cam.ac.uk](mailto:jb511@cam.ac.uk)).

<sup>[C]</sup> Some figures in this article are displayed in color online but in black and white in the print edition.

<sup>[W]</sup> The online version of this article contains Web-only data.

<sup>[OA]</sup> Open Access articles can be viewed online without a subscription.

[www.plantphysiol.org/cgi/doi/10.1104/pp.109.143651](http://www.plantphysiol.org/cgi/doi/10.1104/pp.109.143651)

et al., 1997, 1999). Mutations in the human ortholog ABCB7 are the cause of X-linked sideroblastic anemia with ataxia, in which one of the symptoms is mitochondrial iron overload (Rouault and Tong, 2008). Moreover, ATMs are widespread and highly conserved in  $\beta$ -proteobacteria and could be involved in nickel and cobalt resistance (Mikolay and Nies, 2009).

The Arabidopsis (*Arabidopsis thaliana*) genome contains more than 100 ABC transporters, of which the ATMs form a small subfamily in the B group consisting of three genes: *ATM1*, *ATM2*, and *ATM3* (Rea, 2007). The genes were first identified in Arabidopsis by Kushnir et al. (2001) and were named *STA2*, *STA3*, and *STA1*, respectively. (A proposal for a unified nomenclature [Verrier et al., 2008] has suggested the gene symbols *AtABCB24*, *AtABCB23*, and *AtABCB25* for *AtATM1*, *AtATM2*, and *AtATM3*, respectively. However, for consistency with previous publications, we have adhered to the *ATM* gene symbols in this paper.) Expression of GFP fusions showed that all three ATM proteins localized to mitochondria (Kushnir et al., 2001; Chen et al., 2007). Arabidopsis *ATM3* could functionally complement the yeast *atm1* phenotype (Kushnir et al., 2001; Chen et al., 2007), whereas Arabidopsis *ATM1* complemented poorly and *ATM2* expression was toxic in yeast (Chen et al., 2007). Until now, functional analysis of the *ATM* genes in Arabidopsis has been restricted to one *atm3* mutant, called *starik* (Kushnir et al., 2001), in which the protein lacks the C-terminal ATPase domain. The *atm3-1* (*sta1*) mutant is dwarfed and chlorotic, but the biochemical basis of its pleiotropic phenotypes is unknown. In addition, induced expression of *ATM3* in response to cadmium and lead, as well as sensitivity of the *atm3-1* (*sta1*) mutant to cadmium, have implicated the *ATM3* transporter in heavy metal tolerance (Kim et al., 2006).

We have analyzed a comprehensive set of mutants in the Arabidopsis *ATM* genes and found that *ATM3* plays a key role in plant metabolism, while mutants in *ATM1* and *ATM2* did not display an obvious phenotype. Genetic and biochemical evidence from an *atm3* allelic series showed that *ATM3* is important for the activity of cytosolic Fe-S and molybdenum cofactor (Moco) enzymes, but it does not play a major role in metal homeostasis.

## RESULTS

### ATM3, But Not ATM1 and ATM2, Has a Critical Function under Normal Growth Conditions

To investigate the functions of *ATM1*, *ATM2*, and *ATM3* in Arabidopsis, insertion mutants were obtained from the Arabidopsis stock centers (Fig. 1A; for details, see Table I). Homozygous plants were analyzed by reverse transcription (RT)-PCR, confirming the absence of *ATM1* transcript in the *atm1-1* and *atm1-2* lines and the absence of *ATM3* transcript in the

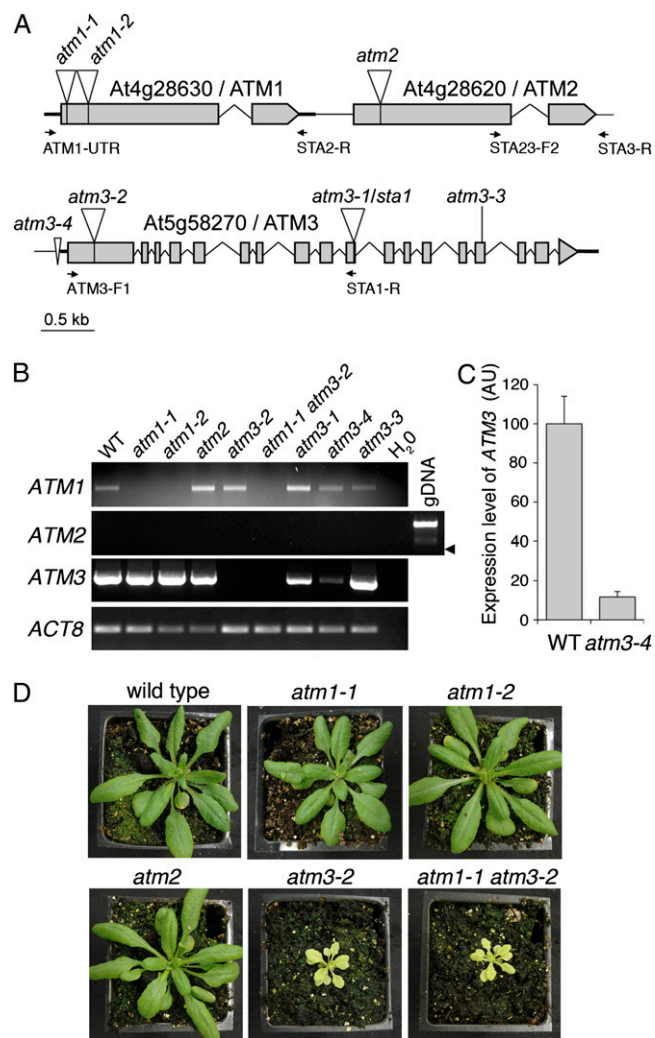


**Figure 1.** Genetic analysis of Arabidopsis mutants in *ATM1*, *ATM2*, and *ATM3*. A, Gene structure of *ATM1*, *ATM2*, and *ATM3* and the positions of T-DNA insertions and other sequence polymorphisms. B, Analysis of *ATM* gene expression by RT-PCR. The positions of the primers are indicated in A. The arrowhead indicates the expected position of the RT-PCR product for *ATM2*. WT, Wild type. C, Quantitative RT-PCR analysis of *ATM3* transcript levels in wild-type and *atm3-4* lines. Error bars indicate  $\text{SD}$  between technical triplicates from one typical experiment. The level of *ATM3* transcripts in the *atm3-4* line was estimated to be  $8.8\% \pm 4.2\%$  of the wild-type level. AU, Arbitrary units. D, Four-week-old individuals of T-DNA insertion lines show that *ATM3*, but not *ATM1* or *ATM2*, is important for plant development under normal conditions. [See online article for color version of this figure.]

*atm3-2* insertion line (Fig. 1B). The expression of *ATM2* in the *atm2* line could not be assessed, as no RT-PCR product of *ATM2* could be detected in the wild type or any other line. However, the *ATM2* primer set gave a positive PCR with genomic DNA. When grown on soil under long-day conditions, the *atm1-1*, *atm1-2*, and *atm2* insertion mutants grew like the wild type, while the *atm3-2* insertion mutant was dwarfed and pale green. The *atm1-1 atm3-2* double mutant was very

**Table I.** Summary of mutant alleles used in this study

Locus	Allele	This Study	Polymorphism	Mutation(s)
AT4G28630 = <i>ATM1</i> , <i>STA2</i>	<i>atm1-1</i>	<i>atm1-1</i>	SALK_090939	T-DNA insertion (+34)
	<i>atm1-2</i>	<i>atm1-2</i>	SALK_121795	Tandem T-DNA insertion (+517)
AT4G28620 = <i>ATM2</i> , <i>STA3</i>	<i>atm2</i>	<i>atm2</i>	WiscDsLox293-296invB11	T-DNA insertion (+498)
AT5G58270 = <i>ATM3</i> , <i>STA1</i>	<i>atm3-1</i> , <i>sta1</i>	$\Delta$ NBD	<i>starik1</i> (Babiychuk et al., 1997)	T-DNA insertion (+1,458) resulting in NPTII fusion protein
	<i>atm3-2</i>	T-DNA	GK-714C03	T-DNA insertion (+426)
	<i>atm3-3</i>	R612K	P25	Point mutation, G-1,835 $\rightarrow$ A
	<i>atm3-4</i>	$\Delta$ prom	M2934	Deletion of -63 to -25

similar to *atm3-2* plants, indicating that *ATM1* plays a minor role compared with *ATM3* (Fig. 1D).

Interestingly, we found new alleles of Arabidopsis *ATM3* in screens for resistance to sirtinol. This compound mimics auxin in the phenotypic responses it causes in plants and has been used for genetic screens that have uncovered mutants in genes involved in auxin signaling (Zhao et al., 2003) and Moco biosynthesis (Dai et al., 2005). Mapping and cloning of the *atm3-3* mutation identified a point mutation (G-1,835 to A) causing a substitution of a highly conserved Arg to Lys (R612K). The *atm3-4* mutant line was allelic with *atm3-3* and was found to have a 39-nucleotide deletion in the promoter extending into the 5' untranslated region, resulting in approximately 90% lower transcript levels as determined by quantitative RT-PCR (Fig. 1C).

The occurrence of *atm3* mutant alleles in genetic screens, higher expression levels, and the strong phenotype of the *atm3-2* insertion mutant indicate that *ATM3* plays a crucial role in plant growth and development, whereas *ATM1* and *ATM2* have negligible functions under normal conditions.

### Phenotypic Analysis of *atm3* Alleles

Next, we focused on the *atm3* mutant alleles to better understand the function of *ATM3* in plants. Together with the previously described *starik* mutant (Kushnir et al., 2001), the sirtinol mutants and insertion mutant formed an allelic series ranging from mild to severe (Fig. 2A). In this paper, the alleles will be indicated by the nature of their mutation to immediately link this to each phenotype, as follows: R612K (Arg-612 to Lys substitution),  $\Delta$ prom (promoter deletion),  $\Delta$ NBD (deletion of the nucleotide-binding domain), and T-DNA (insertion mutant); for further details, see Table I. Inspection of rosette growth showed that only the  $\Delta$ NBD and T-DNA mutants had a dwarfed stature (Fig. 2A). The same mutant alleles were also severely chlorotic, with total chlorophyll levels decreased by more than 50% (Fig. 2B). In contrast, the R612K and  $\Delta$ prom alleles had a more modest but significant 10% decrease in chlorophyll content. Further analysis of the *atm3-1* allele indicated that the lower chlorophyll levels are attributable to lower chloroplast numbers with normal chlorophyll content (Supplemental Fig. S1).

Although the R612K mutant grew as well as the wild type aboveground, the average root length was shortened by nearly 60% in seedlings 8 d after germination (Fig. 2C). The average root lengths of the  $\Delta$ prom,  $\Delta$ NBD, and T-DNA seedlings were even further diminished. The *atm3* alleles were fertile except for the T-DNA (*atm3-2*) mutant, which did not produce seeds (Fig. 2D). Anthers were shrunk and failed to release pollen, but female fertility could be demonstrated in crosses, for instance with *atm1-1* (Fig. 1D).

In addition to the previously described chlorosis and dwarfism (Kushnir et al., 2001), we observed a defect in seedling establishment under low-light conditions. In particular, the R612K,  $\Delta$ NBD, and T-DNA *atm3* alleles showed a decrease in the percentage of seedlings that developed true foliage after 14 d (Fig. 2E). Seedling establishment was fully rescued to wild-type levels by 1% (w/v) Suc in the medium, but addition of Suc did not reverse the chlorosis (data not shown).

Interestingly, the T-DNA insertion mutant, which is likely to represent a null mutant, has a stronger phenotype than the  $\Delta$ NBD mutant. The latter expresses a fusion protein of the membrane domain and neomycin phosphotransferase. If the membrane domain is correctly folded and inserted, this may function as a pore for passive transport of the substrate.

Taken together, broad phenotypic analysis of the *atm3* allelic series shows that chlorosis and decreased root growth are primary defects, while dwarfism and male sterility are probably secondary phenotypes.

### ATM3 Is Required for the Activities of Cytosolic Fe-S Enzymes

To investigate the underlying biochemical causes of the observed phenotypes, we first analyzed the activities of aldehyde oxidases (AO). These enzymes have been implicated to catalyze the conversion of the sirtinol-derivative 2-hydroxy-1-naphthaldehyde to the auxin analog 2-hydroxy-1-naphthoic acid (Dai et al., 2005), and the R612K and  $\Delta$ prom alleles were isolated as sirtinol-insensitive lines. In-gel analysis of AO activities in leaves showed that all three active isoforms were decreased by 10-fold or more in the  $\Delta$ prom,  $\Delta$ NBD, and T-DNA mutants (Fig. 3A; quantification by densitometry not shown). The levels of AO activities

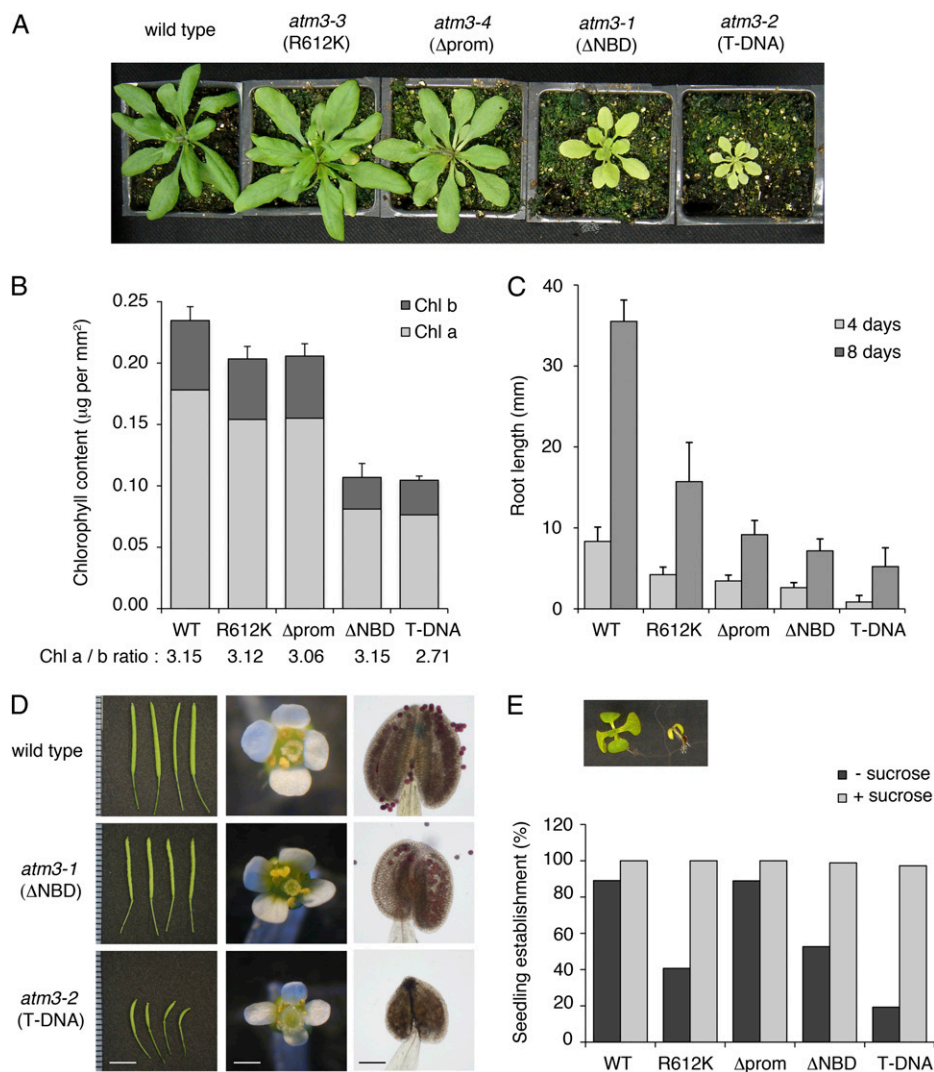


**Figure 2.** Phenotypic analysis of an allelic series of *atm3* mutants. **A**, Rosette growth of the wild type and *atm3* mutant alleles after 4 weeks in 16 h of light/8 h of dark at 20°C. **B**, Chlorophyll (Chl) levels ( $\mu\text{g mm}^{-2}$ ) are decreased in *atm3* alleles. The proportions of chlorophyll *a* and *b* levels are indicated by light and dark gray, respectively, and as numerical values below the graphs.  $n = 6$  for the wild type (WT), R612K, and  $\Delta$ prom;  $n = 4$  for  $\Delta$ NBD;  $n = 3$  for T-DNA. Error bars represent sd. **C**, Root length of wild-type and *atm3* seedlings 4 and 8 d after planting. Seedlings were grown on vertical agar medium containing half-strength Murashige and Skoog medium and 1% (w/v) Suc.  $18 \leq n \leq 23$ , except for the T-DNA line, where  $n = 5$ . Error bars represent sd. **D**, Fertility in the wild type, *atm3-1* ( $\Delta$ NBD), and *atm3-2* (T-DNA) alleles. Bars = 5 mm in the siliques (left), 1 mm in the flowers (middle), and 0.3 mm in the anthers (right). Anthers were stained with Alexander's stain to visualize viable pollen. **E**, The effect of low light (8 h of light/16 h of dark,  $70 \mu\text{mol m}^{-2} \text{s}^{-1}$ ) on the frequency of establishment in wild-type and *atm3* seedlings. Seedlings were grown on Murashige and Skoog medium plus or minus 1% (w/v) Suc and scored for the development of true foliage leaves after 14 d (inset);  $n \geq 50$ .

in the R612K allele of *ATM3* may be decreased slightly, but this is difficult to assess with the semiquantitative in-gel method. In the *atm2* and *atm1-1* mutants, the upper two AO isoforms were similar in activity to the wild type, while the lower isoform was increased in activity. Xanthine dehydrogenase (XDH) activity, an enzyme that is similar in domain structure to AO, was also decreased, correlating with the severity of the *atm3* mutant allele.

AO and XDH are cytosolic enzymes containing two [2Fe-2S] clusters, Moco, and FAD. The first steps of the biosynthetic pathways of both Fe-S clusters and Moco are localized in the mitochondrial matrix (Balk and Lobréaux, 2005; Mendel and Bittner, 2006); therefore, the abundance of either or both cofactors could depend on *ATM3*. To unravel these possibilities, we first measured the activity of nitrate reductase (NR), a cytosolic enzyme depending on Moco, heme, and FAD. NR activity was decreased to about 50% in the  $\Delta$ NBD and T-DNA alleles (Fig. 3B), while the activity

of catalase, a peroxisomal heme-dependent enzyme, was not significantly lower (Fig. 3C). These data may indicate a defect in Moco biosynthesis resulting in a 2-fold decrease in Moco, but this cannot account for the  $\geq 10$ -fold lower AO and XDH activities.

Second, we analyzed the activity of cytosolic aconitase, an enzyme with one [4Fe-4S] cluster. For this purpose, a non-denaturing gel system was developed to separate the three highly similar aconitase isoforms from small leaf samples. The activity was visualized by coupling the aconitase activity to NADP-dependent isocitrate dehydrogenase and the reduction of tetrazolium salt, forming a blue-purple formazan precipitate. Analysis of insertional knockout mutants of *ACO1*, *ACO2*, and *ACO3* showed that the activity with the lowest electrophoretic mobility (the upper band) corresponded to *ACO1* protein (Fig. 4A, left panel). *ACO1*, which lacks a mitochondrial targeting sequence, has previously been shown to provide the majority of aconitase activity in the cytosol (Arnaud

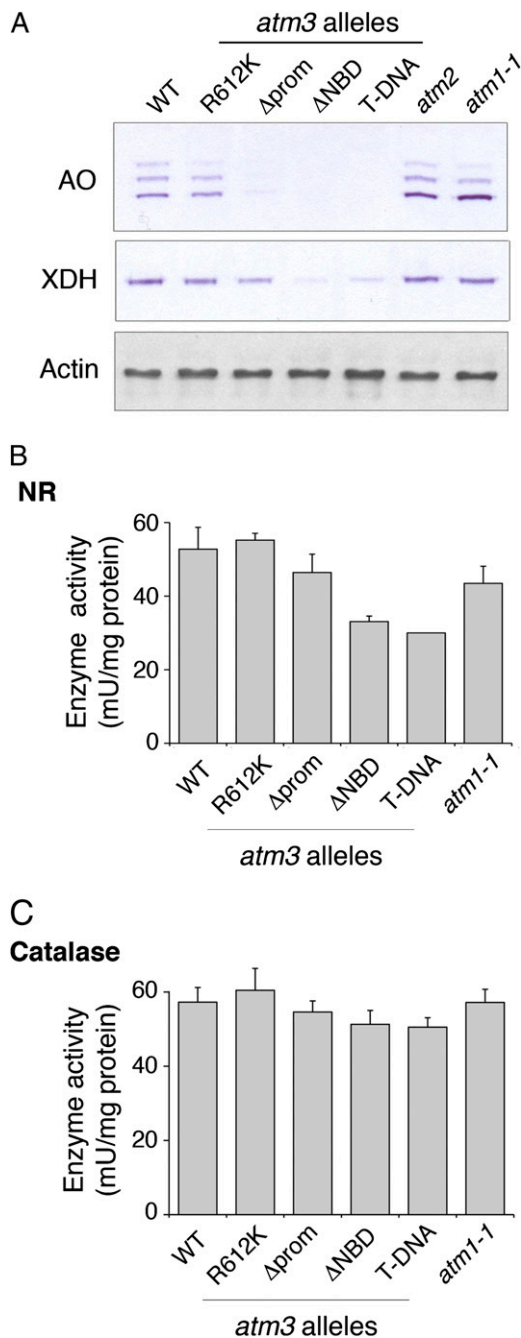


**Figure 3.** ATM3 is required for the activity of Fe-S/Moco enzymes. A, In-gel activities of AO and XDH in the wild type (WT) and *atm* mutants. Equal amounts of protein (60  $\mu$ g) extracted from leaves were separated on nondenaturing PA gels and stained for the indicated enzyme activities using synthetic aldehydes (1-naphthaldehyde and indole-3-carboxyaldehyde) as substrates for AO or hypoxanthine as substrate for XDH. Ten micrograms of protein of the same sample was analyzed by SDS-PAGE and protein-blot analysis for actin as a protein-loading marker. B and C, NR (B) and catalase (C) activities in leaf extracts of the wild type, *atm3*, and *atm1-1* ( $n = 3$  for NR,  $n = 6$  for catalase). Error bars represent SD. [See online article for color version of this figure.]

et al., 2007). Its cytosolic localization was confirmed by protein blot analysis of supernatant and pellet fractions prepared by gentle disruption of leaf protoplasts (Fig. 4A, right panel). ACO2 and ACO3 fractionated in the pellet fraction that contains mitochondria, in agreement with proteomics data (see the SUBA database at <http://www.plantenergy.uwa.edu.au>). Next, we analyzed the in-gel aconitase activities in wild-type and *atm* leaves. The cytosolic ACO1 activity was strongly decreased in *atm3* mutant alleles, whereas the mitochondrial aconitase activities were equal (Fig. 4B, top panel; note that the ACO3 activity is low relative to its protein abundance). The intensity of activity staining of ACO1 was decreased by approximately 20% in R612K, 40% in  $\Delta$ prom, and 60% in  $\Delta$ NBD (see quantification in Supplemental Fig. S2). The decrease in ACO1 activity was paralleled by the abundance of holoprotein, as shown by protein-blot analysis of the native gel (Fig. 4B, middle panel). In contrast, the transcript levels of *ACO1* were equal in all *atm3* alleles (Fig. 4C).

To corroborate the in-gel aconitase results, cytosolic and mitochondrial fractions were prepared from root callus. Photometric enzyme analysis showed a decrease in aconitase activity in the cytosolic fractions of the *atm3* lines, correlating with the severity of the *atm3* mutation, but similar mitochondrial aconitase activity (Fig. 4D). At first, the magnitude of decrease seemed less than that observed in-gel, but we found that a large proportion of the aconitase activity in the cytosolic fraction can be attributed to contamination with mitochondrial matrix proteins. The activity of fumarase, an exclusively mitochondrial enzyme, was approximately 20% in the cytosolic fractions of all *atm3* callus lines, which would correspond to 40 milliunits  $\text{mg}^{-1}$  aconitase activity from mitochondrial origin (Fig. 4D, indicated by the asterisk). Subtracting this showed that the actual cytosolic aconitase activity was decreased by approximately 30% in the  $\Delta$ prom and by approximately 70% in the T-DNA insertion mutant, corresponding to the in-gel analysis. The activities of cytosolic AO and XDH were also decreased in the callus lines (data not shown). In summary, ATM3 is primarily required for the activity of cytosolic Fe-S enzymes and to some extent for Moco enzymes but not for heme-dependent enzymes.

#### ATM3 Is Not Required for Mitochondrial and Plastid Fe-S Enzymes

To further investigate the impact of ATM3 mutations on organellar Fe-S proteins, key enzymes and processes that are dependent on Fe-S clusters were analyzed in the mitochondria and plastids. First, electron transfer from succinate to cytochrome *c*, using complex II (three Fe-S clusters) and complex III (one Rieske-type Fe-S cluster, heme) of the mitochondrial respiratory chain, was measured in callus mitochondria. Cytochrome *c* reduction rates were similar in

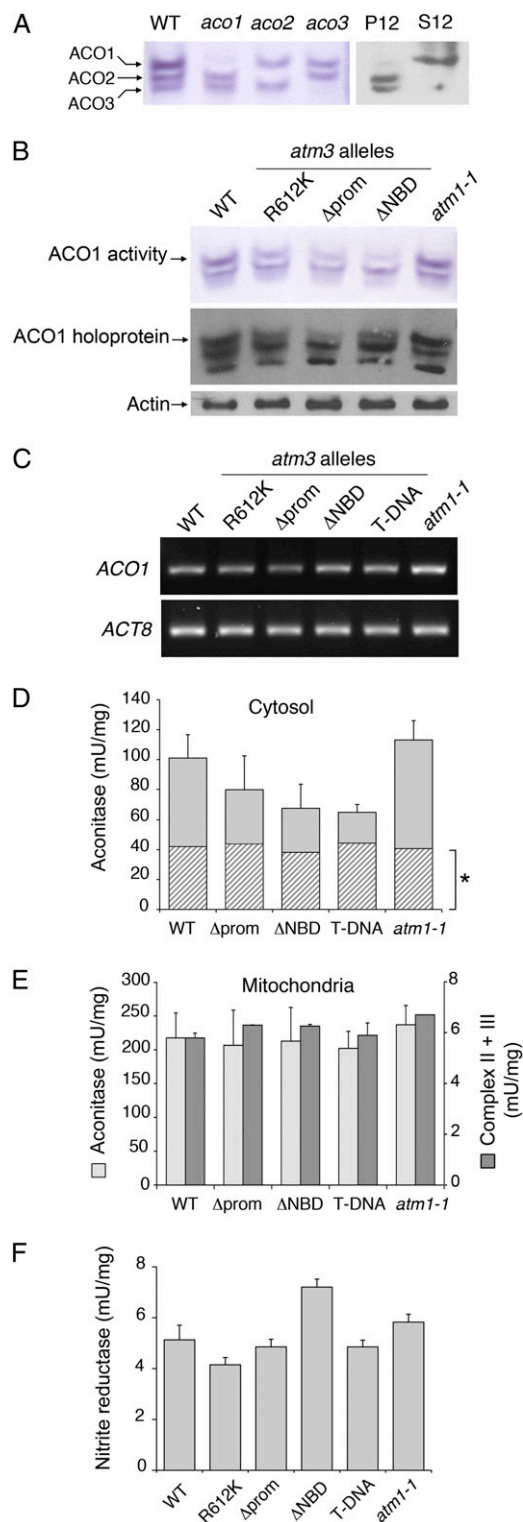


**Figure 4.** ATM3 is required for the activity of cytosolic aconitase but not mitochondrial and plastid Fe-S enzymes. A, In-gel activities and protein blots of Arabidopsis aconitase isoforms in the wild type (WT) and *aco* mutants. Equal amounts of protein (80  $\mu$ g) extracted from leaves were separated on nondenaturing gels containing 2% (w/v) starch/8% (w/v) PA in Tris-borate buffer and stained for aconitase activity (purple) as described in "Materials and Methods." In addition,

*atm3* alleles, *atm1-1*, and wild-type mitochondria (Fig. 4E). Second, leaf extracts were analyzed for the activity of nitrite reductase (NiR), a Fe-S- and heme-dependent enzyme exclusively localized in the plastids. NiR activity was not decreased in the *atm3* phenotypic series (Fig. 4F), although variations in its activity occurred, most notably an increase in NiR activity in  $\Delta$ NBD correlating with lower NR activity (Fig. 3B).

To assess the function of Fe-S proteins in the photosynthetic machinery, fluorescence and P700 absorbance parameters were recorded with a Dual-PAM-100 measuring system in intact leaves (Table II). P700 oxidation ( $\Delta A_{820}/A_{820}$ ) was halved in *atm3-1* ( $\Delta$ NBD) and decreased to one-third in *nfu2.1* compared with the wild type. However, when normalized to chlorophyll content, the P700 absorbance change in *atm3-1* was similar to that in the wild type, in agreement with normal PSI activity measured in isolated chloroplasts (Supplemental Fig. S3). In the *nfu2.1* mutant, in contrast, normalized P700 absorbance was 2-fold lower than in the wild type, reflecting the lower PSI levels reported previously (Touraine et al., 2004; Yabe et al., 2004). Furthermore, a 3-fold increase of the parameter Y(NA) indicated that P700 oxidation in *nfu2.1* is acceptor limited (i.e. P700 cannot be oxidized by a saturation pulse due to a lack of available electron acceptors, including ferredoxin [2Fe-2S]). In contrast, no P700 acceptor-side limitation is observed in *atm3* mutants.

Taken together, the normal activity of key mitochondrial and plastid Fe-S enzymes indicates that ATM3 is not required for Fe-S cluster assembly in these organelles.

#### ATM3 Plays a Minor Role in Metal Homeostasis

In yeast and human, dysfunction of Atm1p and ABCB7, respectively, leads to constitutive expression of iron-uptake genes and accumulation of iron in the mitochondria (Lill and Mühlenhoff, 2008; Rouault and Tong, 2008). To investigate whether this is the case in

leaf protoplasts were disrupted and centrifuged at 12,000g to obtain pellet (P12) and supernatant (S12) fractions enriched in mitochondrial and cytosolic proteins, respectively. After separation on starch/PA gels, the fractions were blotted and labeled with aconitase antibodies (gray scale). B, In-gel aconitase activities (purple) and protein levels (gray scale) in wild-type, *atm3*, and *atm1-1* leaves. For quantification, see Supplemental Figure S2. An equal volume (5  $\mu$ L) of the native sample was separated on a denaturing gel, blotted, and labeled for actin as a loading control. C, RT-PCR of *ACO1* and *ACT8* in wild-type, *atm3*, and *atm1-1* leaves. D and E, Activities of Fe-S enzymes in the cytosolic fraction (D) and purified mitochondria (E) of callus generated from roots of wild-type, *atm3*, and *atm1-1* seedlings ( $n = 3$ ). Based on fumarase activity measurements, approximately 40 milliunits of aconitase in the cytosolic fraction is estimated to be of mitochondrial origin (indicated by the asterisk). Error bars represent s.d. F, NiR activity in leaf extracts of the wild type, *atm3*, and *atm1-1* ( $n = 3$ ). Error bars represent s.d.

**Table II.** Chlorophyll fluorescence of PSII, redox state of P700 (PSI), and acceptor-side limitation in the wild type, *atm3* mutants, and *nfu2.1**atm3-2* leaves were too small for analysis. The values represent means of four measurements  $\pm$  SD.

Allele	PSII		PSI		Acceptor-Side Limitation Y(NA)
	$F_v/F_m$	$\Delta A_{820}/A_{820}$ ( $\Delta I/I \times 10^{-3}$ )	$\Delta A_{820}/A_{820}$ Normalized to Chlorophyll per Leaf Area		
Wild type (Col-0)	0.79 $\pm$ 0.005	4.94 $\pm$ 0.65	4.94 $\pm$ 0.65		0.06 $\pm$ 0.02
<i>atm3-3</i> (R612K)	0.78 $\pm$ 0.006	4.44 $\pm$ 0.77	5.21 $\pm$ 0.90		0.06 $\pm$ 0.02
<i>atm3-4</i> ( $\Delta$ prom)	0.79 $\pm$ 0.007	4.67 $\pm$ 0.35	5.25 $\pm$ 0.39		0.06 $\pm$ 0.02
<i>atm3-1</i> ( $\Delta$ NBD)	0.74 $\pm$ 0.007	2.45 $\pm$ 0.11	4.72 $\pm$ 0.21		0.06 $\pm$ 0.01
<i>nfu2.1</i>	0.58 $\pm$ 0.035	1.38 $\pm$ 0.52	2.66 $\pm$ 0.10		0.20 $\pm$ 0.04

*atm3* mutants in Arabidopsis, the expression of two iron-regulated genes, encoding the root iron transporter IRT1 and ferritin, was analyzed at the protein level in the *atm3-1* ( $\Delta$ NBD) mutant. Seedlings were grown on minimal medium with 1, 10, 20, and 40  $\mu$ M iron. As expected, the levels of IRT1 in wild-type roots were strongly increased under iron-limiting conditions (1  $\mu$ M iron) but nondetectable under iron-replete conditions (10  $\mu$ M iron and higher; Fig. 5A, top panels). In *atm3-1* roots, IRT1 was also strongly induced under iron-limiting conditions, but contrary to the wild type, low levels of the protein were detectable at 10 and 20  $\mu$ M iron. Ferritin levels in roots correlated inversely with those of IRT1 (Fig. 5A, top panels). In particular, *atm3-1* roots had lower ferritin levels than the wild type, corresponding to attenuated IRT1 expression at 10 to 20  $\mu$ M medium iron. At 40  $\mu$ M medium iron, ferritin levels were approximately 2-fold lower in *atm3-1* roots compared with the wild type (densitometric quantification). In rosette leaves, the levels of ferritin increased with the iron concentration in the medium (Fig. 5A, bottom panels) but were overall 1.5 times less in *atm3-1* leaves, correlating with lower chlorophyll content and chloroplast numbers (Fig. 2B; Supplemental Fig. S1). Taken together, the expression patterns of IRT1 and ferritin in the *atm3-1* mutant are not constitutive but generally respond to external iron levels. Nevertheless, the attenuated IRT1 and ferritin levels suggest that *atm3-1* seedlings may experience a mild iron deficiency.

Next, the iron content of mitochondria was measured in purified organelle preparations. Neither mitochondria from *atm3* callus lines nor from *atm3-1* ( $\Delta$ NBD) leaves contained elevated levels of iron (Fig. 5B). Although Kushnir et al. (2001) found 1.5 to 1.8 times more iron in mitochondria purified from *atm3-1* (*sta1*) cell culture, both results are clearly different from yeast cells upon down-regulation of *ScATM1*, where iron levels are increased at least 10-fold (Fig. 6D) and could cause the loss of cytochromes and mitochondrial DNA (Kispal et al., 1999). Chloroplast iron levels were also not altered in the *atm3-1* mutant (Fig. 5B).

Furthermore, it was investigated whether the phenotype of *atm3-1* seedlings could be alleviated by applying iron directly to the leaves, bypassing uptake

and xylem transport. While spraying with ferric ammonium significantly improved growth and chlorophyll biosynthesis in the *irt1-1* mutant (Varotto et al., 2002), this treatment had no effect on *atm3-1* seedlings (Fig. 5C). Either the *atm3* mutants cannot use iron properly, resulting in functional iron deficiency, or the chlorosis is not caused by iron deficiency.

Following a report that the *atm3-1* mutant roots showed a growth reduction in the presence of cadmium (Kim et al., 2006), the effect of cadmium on root length was tested for all *atm3* alleles. Under our conditions, cadmium concentrations of 20 to 40  $\mu$ M inhibited root growth in all *atm3* alleles to a similar extent as in the wild type (Fig. 5D, top). When the data are rendered as a percentage of wild-type root length, root growth is only slightly more inhibited by cadmium in *atm3* alleles than in the wild type (Fig. 5D, bottom). The effect of cadmium observed by Kim et al. (2006) in the *atm3-1* mutant (C24 background) is also relatively weak (85% growth reduction in the mutant compared with 49% in the wild type) and very minor compared with that observed for mutants in the bona-fide cadmium extrusion pump AtPDR8 (Kim et al., 2007). These data suggest that ATM3 may play an indirect, rather than a direct, role in heavy metal resistance.

In summary, metal homeostasis is only marginally affected in *atm3* mutants, supporting the general view that iron regulation differs in plants from fungi/metazoa (Curie and Briat, 2003). Importantly, iron sensing may not depend on a Fe-S cluster protein as in yeast and mammals (Lill and Mühlenhoff, 2008).

#### Arg-612 Has a Conserved Function in B-Group ABC Transporters

To confirm the effect of the R612K substitution in ATM3, especially since AO activities were not dramatically decreased in the Arabidopsis mutant (Fig. 3A), we engineered the equivalent amino acid substitution in yeast Atm1p (R569K). The Arg is strictly conserved in all ATM protein sequences, although it can be a Lys, Ala, or Gly in other ABC transporters (Supplemental Fig. S4). Comparison with the Sav1866 structural model showed that Arg-612 (Arg-569 in yeast Atm1p) is located on the so called x-loop connecting the membrane domain and the ATPase

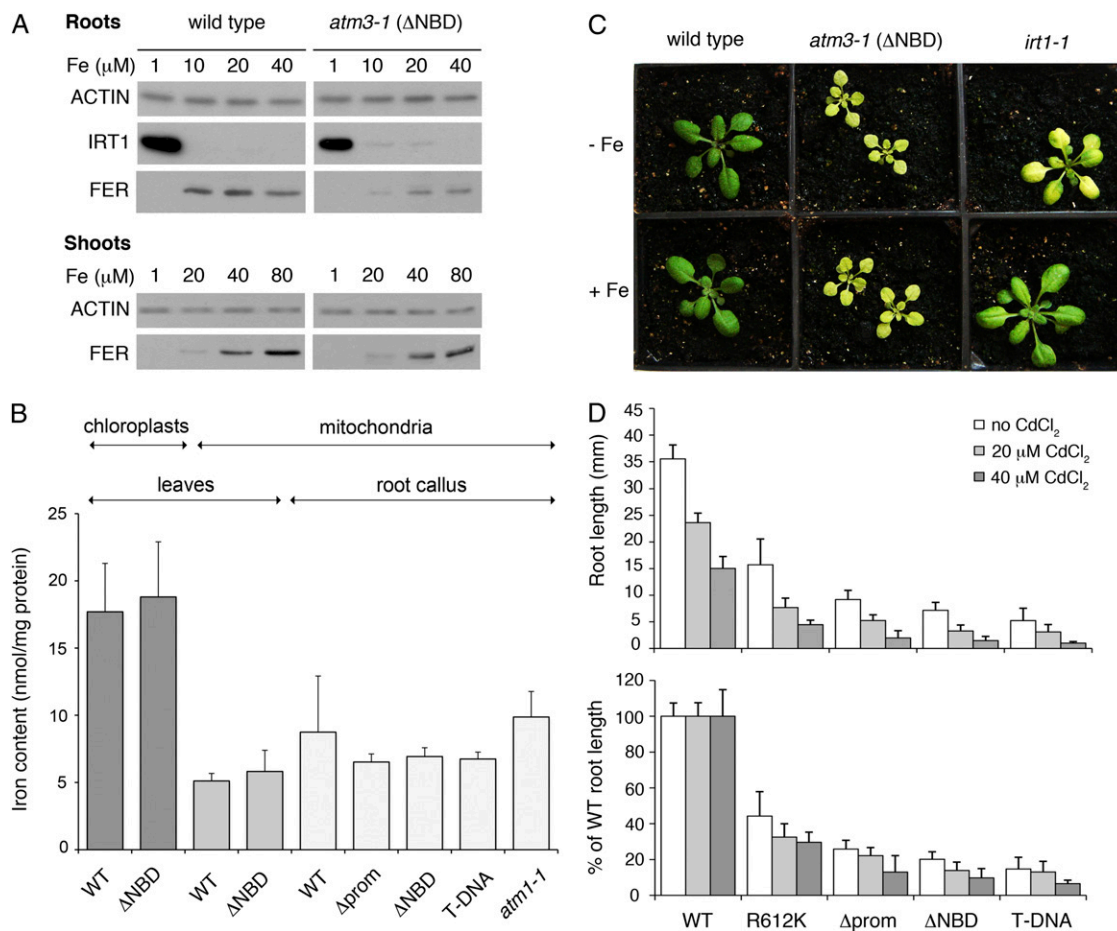


**Figure 5.** ATM3 plays a minor role in metal homeostasis. A, IRT1 and ferritin levels in response to iron. Wild-type and *atm3-1* seedlings were germinated on minimal nutrient medium with 1, 10, 20, and 40 (80)  $\mu\text{M}$  NaFeEDTA. After 17 d, protein extracts of roots or shoots were analyzed by immunoblot analysis with antibodies against the iron transporter IRT1 or ferritin. B, Iron content in organelles isolated from root callus or rosette leaves. Total iron was measured in samples of 150  $\mu\text{g}$  of mitochondrial proteins using a colorimetric assay with the iron chelator ferene ( $n = 4$  for purified leaf mitochondria,  $n = 2$  for callus mitochondria) or in samples of 2 to 3 mg of chloroplast protein by inductively coupled plasma-mass spectrometry following nitric acid digestion ( $n = 3$ ). Error bars represent sd. C, Spraying with iron ammonium citrate does not rescue the chlorosis of the *atm3-1* ( $\Delta\text{NBD}$ ) mutant. The *irt1-1* mutant line was used for comparison. D, *atm3* mutants display a minor sensitivity to cadmium. Seedlings were grown on vertical agar medium containing half-strength Murashige and Skoog medium and 1% (w/v) Suc, without or with 20 or 40  $\mu\text{M}$  CdCl<sub>2</sub>, as indicated. Root length was measured 8 d after planting.  $12 \leq n \leq 23$ , except for the T-DNA line, where  $5 \leq n \leq 7$ . Error bars represent sd. WT, Wild type. [See online article for color version of this figure.]

domain (Dawson and Locher, 2006). We expressed mutant versions of *ScATM1* from a p426 plasmid in cells in which the endogenous *ATM1* gene is under the control of the *GAL1-10* promoter, which is activated by Gal but repressed by Glc or lactate (Kispal et al., 1999). Depletion of endogenous *Atm1p* strongly decreased the growth of cells containing the empty vector, whereas production of the R569K- or R569A-substituted proteins maintained growth (Fig. 6A). Protein blot analysis showed that the amino acid substitutions did not affect the stability of *Atm1p* (Fig. 6B).

Next, we analyzed the effect of the R569K and R569A substitutions in *Atm1p* on the activity of two cytosolic Fe-S enzymes, isopropyl malate isomerase (the second step in Leu biosynthesis) and sulfite reductase. Interestingly, Lys substitution of Arg-569

resulted in an approximately 50% decrease of both activities, whereas Ala substitution had little effect (Fig. 6C). The activity of alcohol dehydrogenase (ADH), a zinc-dependent enzyme that was analyzed as a control, was not altered in the mutants compared with wild-type *ATM1*. Note that ADH activity is strongly increased in the empty-vector control, because *Atm1p*-depleted cells switch their metabolism to alcohol fermentation (Kispal et al., 1997).

To investigate mitochondrial iron accumulation, cells were grown with Glc or with lactate to deplete endogenous *Atm1p*, and mitochondria were purified by differential centrifugation. In the presence of Glc, little iron accumulated in mitochondria, as reported previously (Kispal et al., 1999). However, in the presence of lactate, a nonfermentative carbon source that

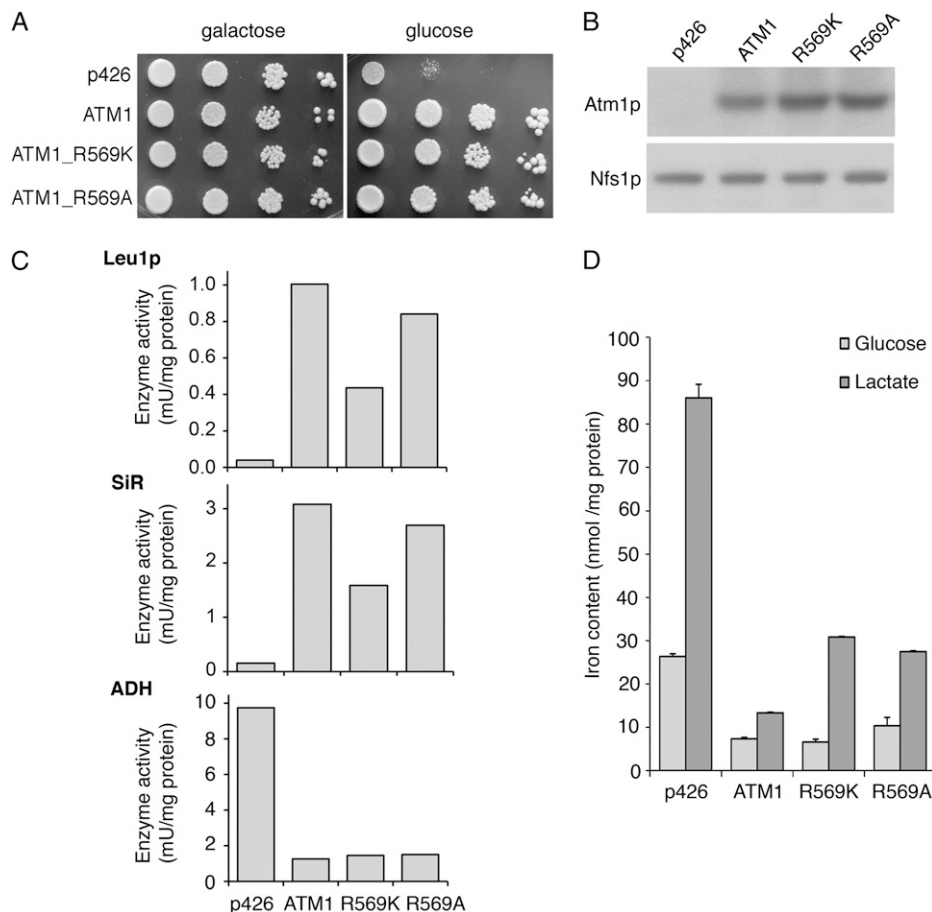


**Figure 6.** Arg-569 to Lys substitution in yeast Atm1p results in impaired activity of cytosolic Fe-S proteins. A, Ten-fold serial dilutions of Gal-ATM1 cells transformed with p426, p426-ATM1, p426-ATM1\_R569K, or p426-ATM1\_R569A were grown on minimal medium containing Gal or Glc as a carbon source and incubated at 30°C for 4 d. B, R569K and R569A substitutions do not modify the stability of Atm1p. Immunoblot analysis of Atm1p or Nfs1p (as a loading control) in mitochondria purified from cells as described in A grown on Glc. C, The activities of isopropyl malate isomerase (Leu1p) and sulfite reductase (SiR) are decreased when Arg-569 is replaced by a Lys in Atm1p. Enzyme activities were measured using cell extracts prepared from cells described in A grown in the presence of Glc to deplete endogenous Atm1p. ADH activity was monitored as a control. Graphs represent data from one typical experiment (repeated three times with reproducible results). D, Iron accumulation in mitochondria from cells expressing mutant versions of *ATM1*. Yeast cells as described in A were grown in minimal Glc or rich lactate medium. Iron content was measured in samples of 150  $\mu$ g of mitochondrial protein using the colorimetric iron chelator ferene ( $n = 2$ ). Error bars represent SD.

requires mitochondrial respiration, approximately 10-fold more iron was associated with mitochondria from Atm1p-depleted cells (p426; Fig. 6D). A 2-fold increase in mitochondrial iron content was observed in the R569K and R569A mutants.

These results show the importance of the x-loop Arg for the function of eukaryotic ATM proteins. Clearly, the positive charge of this residue is not critical, but the Arg performs a specific role in ATM proteins, at the interface of the membrane domain to ATP hydrolysis.

## DISCUSSION

Arabidopsis has three closely related *ATM* genes, whereas other plant species like rice (*Oryza sativa*) and

yeast have only one gene (Chen et al., 2007). Here, we show that only mutations in *ATM3* affected plant growth, while T-DNA insertions into *ATM1* and *ATM2* did not result in an obvious phenotype (Fig. 1C). The T-DNA insertions in *atm1-2*, *atm2*, and *atm3-2* lines are all in a similar position at the 5' end of the open reading frame, corresponding to the first transmembrane helix. Therefore, it is unlikely that partial transcription of *ATM1* or *ATM2*, but not *ATM3*, could lead to a functional protein. We investigated whether the function of *ATM1* allowed slow growth of the *atm3-2* mutant, but mutation of *atm1-1* in the *atm3-2* background did not further enhance the phenotype of *atm3-2* (Fig. 1D). Likewise, *atm2 atm3-1* double mutants resembled the *atm3-1* parental line (data not shown). Either the expression levels of *ATM1* and

*ATM2* are too low to compensate for the absence of *ATM3* (Fig. 1B; Chen et al., 2007) or sequence divergence prevents complementation of *atm3*. Both arguments may be valid. First, accumulated microarray data suggest that the combined mRNA levels of *ATM1* and *ATM2*, which are not listed separately because of high sequence identity, are approximately 5% of *ATM3* (Genevestigator). Moreover, the expression of *ATM1* or *ATM2* is not up-regulated in the *atm3-2* mutant (Fig. 1B). Second, Kushnir and colleagues (2001) showed that overexpression of *ATM1* (*STA2*) from the 35S promoter did not rescue the pleiotropic phenotypes of *atm3-1* (*sta1*), although it did improve growth. Taken together, our data and those of others suggest that *ATM3* is likely to function as a homodimer rather than a heterodimer with *ATM1* or *ATM2*. It is further of interest that *ATM3* is not essential for viability (assuming that *atm3-2* is a true null mutant; Fig. 1D). Yeast *ATM1* also is not an essential gene, despite the fact that a number of cytosolic/nuclear Fe-S proteins are essential (Lill and Mühlenhoff, 2008). It has been suggested that other mitochondrial ABC transporters have overlapping substrate specificities with AtATM3/ScAtm1p or that some membrane diffusion of the substrate can occur. The mammalian ortholog ABCB7, on the other hand, is essential for early embryonic development in mice (Pondarré et al., 2006).

How can the phenotypes of the *atm3* mutant alleles be explained? Slow root growth can be the result of many biochemical defects, not in the least in plant hormone biosynthesis. The identification of weak *atm3* alleles in sirtinol screens suggests lower activities of AO, as confirmed in the *atm3-4* allele, which will affect abscisic acid and possibly auxin biosynthesis (Mendel and Bittner, 2006). Indeed, abscisic acid levels are strongly decreased in *atm3-1* mutants and do not respond to drought treatment (J. Teschner and F. Bittner, unpublished data). Poor seedling establishment in *atm3* alleles (Fig. 2E) may be the consequence of impairment of the glyoxylate cycle (Eastmond et al., 2000), due to lower activities of cytosolic aconitase (Fig. 4, B and D). However, the percentage of seedling establishment did not correlate fully with the levels of cytosolic aconitase activity in the *atm3* alleles, and other factors may affect this biological process.

As more and more Fe-S enzymes are being identified, especially in DNA repair, transcription, and translation (for review, see Lill and Mühlenhoff, 2008), it is no surprise that *ATM3*, which we show is primarily important for the function of cytosolic (and by extension nuclear) Fe-S enzymes, is important for many aspects of plant metabolism. For example, the previously observed 2- to 10-fold up-regulation of DNA repair enzymes (Kushnir et al., 2001) could be a response to lower activities of Fe-S-dependent analogs (Balk and Lobréaux, 2005). However, so far we have been unable to explain why *atm3* mutants are chlorotic. The chloroplasts, although much lower in number, appear normal in *atm3-1* (*sta1*), with extensively developed thylakoid membranes stacked into granas

(Kushnir et al., 2001), corresponding to mostly unaltered enzyme activities and photosynthesis parameters (Fig. 4F; Table II; Supplemental Fig. S3). Furthermore, chlorophyll levels and iron content in isolated chloroplasts are similar in *atm3-1* and the wild type. Together with only subtle changes in the expression of iron-regulated genes (Fig. 5A) and no effect of foliar iron application (Fig. 5C), it also seems unlikely that the chlorosis is caused by iron deficiency. Therefore, we hypothesize that an as yet unknown cytosolic or nuclear Fe-S protein is important for developing full photosynthetic capacity in the leaves. Alternatively, there is a possibility that the substrate of *ATM3* is required for a specific plastid function, other than Fe-S cluster assembly by the stromal assembly machinery. This would implicate plastid localization of *ATM3*, for which there is indeed some proteomic evidence. In addition to studies confirming mitochondrial localization (Brugière et al., 2004; Heazlewood et al., 2004), *ATM3* has been found in two proteomic studies of the plastids (Froehlich et al., 2003; Zybailov et al., 2008) but not in the study of Ferro et al. (2003). GFP and immunological studies are currently being undertaken in our laboratory to revisit the previously published GFP localization data (Kushnir et al., 2001; Chen et al., 2007) and to investigate whether a minor fraction of *ATM3* is dual localized.

Our data provide fresh clues about the substrate of *ATM3* that will form the basis for future investigations. Although *ATM3*, and therefore the substrate, is required for cytosolic Fe-S clusters, it is unlikely to be an Fe-S cluster. First, free Fe-S is unstable and would need to be liganded, for instance by a small peptide (Kuhnke et al., 2006). Second, iron does not accumulate in the mitochondria of *atm3* mutants (Fig. 6C). Possibly, *ATM3* could transport a chemical form of sulfur, generated by the mitochondrial Cys desulfurase NFS1, which then assembles with iron in the cytosol to form Fe-S clusters, mediated by the cytosolic Fe-S assembly machinery. Persulfide from Cys desulfurases, rather than hydrogen sulfide generated by sulfite reductase, appears to be the form of sulfur required for Fe-S cluster assembly (Kessler, 2006). It is interesting in this respect that the activity of NR, a Moco enzyme, is decreased in *atm3* mutants. *ATM3* may also provide sulfur to the second step of Moco biosynthesis localized in the cytosol (Dai et al., 2005; Mendel and Bittner, 2006). However, other possibilities cannot be ruled out, for example that *ATM3* transports multiple substrates, including the pterin precursor of Moco. In support of a sulfide derivative as substrate, it was shown that the ATPase activity of yeast Atm1p is stimulated by thiol compounds in vitro (Kuhnke et al., 2006). Although it has been suggested that *ATM3* transports cadmium, our finding that cadmium has little effect on root length in *atm3* mutants (Fig. 6D) does not support this idea.

The analysis of *ATM3* sheds further light on the compartmentalization of Fe-S cluster assembly in plant cells and the cross talk between these pathways

(Xu and Møller, 2008). While ATM3 links the mitochondrial ISC machinery with the cytosol, Fe-S cluster assembly in the plastids appears to be an independent process.

## MATERIALS AND METHODS

### Plant Material and Growth

*Arabidopsis* (*Arabidopsis thaliana*) ecotype Columbia (Col-0) was used as the wild type and the background of all mutants used in this study. The following insertion mutants were obtained from the Nottingham Arabidopsis Stock Centre: SALK\_090939 and SALK\_121795, named *atm1-1* and *atm1-2*, respectively, for the *ATM1* gene (AT4G28630); N850573, named *atm2*, for the *ATM2* gene (AT4G28620); and GK-714C03, named *atm3-2*, for the *ATM3* gene (AT5G58270). The *atm3-2* mutant was maintained as a heterozygous line segregating in a 1:3 ratio. The presence and positions of the T-DNAs were confirmed by PCR. The *starik* mutant (in ecotype C24) was a kind gift from Sergei Kushnir. The line was backcrossed into Col-0 and renamed *atm3-1*. The sirtinol-resistant *atm3-3* and *atm3-4* mutations were cloned using a map-based positional cloning approach (Dai et al., 2005). A total of 1,584 F2 individuals for *atm3-3* and 2,367 F2 individuals for *atm3-4* were used. The mutations responsible for sirtinol resistance were mapped to a 90-kb mapping interval on bacterial artificial chromosomes K21L19 and MCK7. The G-1,835 to A mutation in *atm3-3* and the -63 to -25 deletion in *atm3-4* were identified by sequencing. Allelism of all four *atm3* mutants was confirmed by crosses (data not shown).

The *aco1*, *aco2*, *aco3*, and *nfu2.1* mutant lines (GK-138A08, SALK\_014661, SALK\_054196, and SALK\_039254, respectively) were obtained from the Nottingham Arabidopsis Stock Centre and have been described previously (Touraine et al., 2004; Yabe et al., 2004; Arnaud et al., 2007; Moeder et al., 2007).

Plants were grown on compost in 16-h-light/8-h-dark cycles with a photon flux density of  $140 \mu\text{mol m}^{-2} \text{s}^{-1}$  at 20°C and 60% humidity, unless otherwise stated. Callus was generated from roots as described previously (Prime et al., 2000).

### Yeast Strains and Growth

*Saccharomyces cerevisiae* strain W303-1A (*MATa*, *ura3-1*, *ade2-1*, *trp1-1*, *his3-11,15*, *leu2-3 112*) served as the wild type. The Gal-*ATM1* (*HIS3*) strain, in which *ATM1* is under the control of the Gal-inducible promoter *GAL1-10*, was described previously, as well as conditions for depletion of Atm1p (Kispal et al., 1999). Mutagenesis of *ScATM1* was performed using the QuikChange Site-Directed Mutagenesis Kit from Stratagene, using the plasmid pRS426-*ScATM1* as a template and primers as specified in Supplemental Table S1. Yeast cells were transformed by the lithium acetate procedure (Schiestl and Gietz, 1989).

### RT-PCR

Total RNA was extracted from leaves using TRIzol reagent, followed by purification on a Qiagen RNA purification column, according to the manufacturer's instructions. RT was performed with oligo(dT) and RevertAid H<sup>-</sup> Moloney murine leukemia virus reverse transcriptase (Fermentas) using 2.4  $\mu\text{g}$  of total RNA. cDNAs were PCR amplified using the following gene-specific primers: ATM1-UTR and STA2-R for *ATM1*, STA23-F2 and STA3-R for *ATM2*, ATM3-F1 and STA1-R for *ATM3*, ACO1-F1 and ACO1-R2 for *ACO1*, and ACT8-F and ACT8-R for *ACT8* (Fig. 1A; Supplemental Table S1). To discriminate PCR products resulting from cDNA and contaminating genomic DNA, primers were designed to span at least one intron. Note that the discrepancy in RT-PCR results for *ATM2* with Chen et al. (2007) could be due to their choice of primers, which did not rule out PCR products arising from genomic DNA, or to being close to the limit of detection.

For quantitative RT-PCR, the *ATM3* and *ACT8* products were amplified with primers ATM3-R1/ATM3-F3 and ACT8-R/ACT8-F, respectively, using cDNAs prepared from Col-0 and *atm3-4* lines as a template. PCR amplification was carried out in the presence of the double-stranded DNA-specific dye SYBR Green (Sigma) and monitored in real time with a Bio-Rad Chrom4 qPCR machine. Difference in *ATM3* mRNA abundance was deduced from the cycle threshold values, using *ACT8* expression levels for normalization.

### Enzyme Assays

In-gel activity assays for aldehyde oxidases and XDH were performed as described previously (Koshiba et al., 1996). For in-gel analysis of aconitase activities, proteins were extracted by grinding 50 to 100 mg of leaf tissue with 1.5 volumes of 50 mM Tris-HCl, pH 8.0, 50 mM KCl, 0.2% (v/v) Triton X-100, 2 mM sodium citrate, and 1 mM dithiothreitol. Samples were centrifuged for 15 min at 4°C at maximum speed in a microfuge. The supernatant was mixed with 0.25 volume of loading buffer (20 mM Tris-HCl 8.0, 80% [v/v] glycerol, and 0.1% [w/v] bromophenol blue), and 80 to 100  $\mu\text{g}$  of protein was loaded per lane. The proteins were separated on a minigel with a stacking gel of 4% (w/v) polyacrylamide (PA) and a running gel of 2% (w/v) hydrolyzed potato starch (Starch Art), 8% (w/v) PA in 0.13 M Tris-borate buffer, pH 8.6, and 3.6 mM sodium citrate. Gels were run in 0.025 M Tris-Gly buffer, pH 8.3, and 3.6 mM sodium citrate at 120 V for 3.5 h. The activity of aconitases was visualized by incubating the gels in 0.1 M Tris-HCl, pH 8.0, 2.5 mM MgCl<sub>2</sub>, 0.5 mM NADP, 2.5 mM cis-aconitase, 5 mg mL<sup>-1</sup> thiazolyl blue tetrazolium bromide, 50  $\mu\text{g}$  mL<sup>-1</sup> phenazine methosulfate, and 0.13 units mL<sup>-1</sup> porcine isocitrate dehydrogenase for 10 to 30 min at room temperature.

Aconitase activity in cell extracts and mitochondria was assayed by coupling the activity to isocitrate dehydrogenase and the formation of NADPH (Stehling et al., 2007). Fumarase activity was measured following the conversion of L-malate (50 mM) into fumarate at 240 nm. Complex II (succinate dehydrogenase) and complex III activities were assayed as the reduction of cytochrome *c* at 550 nm after addition of succinate (12 mM) in intact mitochondria (Stehling et al., 2007). For catalase, the disappearance of hydrogen peroxide (12.5 mM) was monitored at 240 nm. NR activity was measured following nitrite production, detected as in the NiR activity assay (Takahashi et al., 2001). The yeast enzymes isopropyl isomerase and sulfite reductase were assayed as described previously (Kispal et al., 1999; Rutherford et al., 2005).

### Cell Fractionation and Protein-Blot Analysis

Cytosolic and mitochondria-enriched fractions were prepared from protoplasts and callus according to Somerville and Ogren (1981) and Sweetlove et al. (2007), respectively, except that differential centrifugation steps were deemed to give sufficient purity and density gradients were omitted. Mitochondria were purified from leaves following Day et al. (1985) and from yeast according to Daum et al. (1982). Chloroplasts were isolated following the method of Aronsson and Jarvis (2002). Protein concentrations were determined with Coomassie Dye Reagent (Bio-Rad). Proteins were separated by PA gel electrophoresis, transferred to nitrocellulose membrane by electroblotting, and labeled with antibodies and chemiluminescence detection. Polyclonal antibodies against purified His-AtACO1 (amino acids 120–898) were raised in rabbit courtesy of Sabine Molnik and Roland Lill. Antibodies against IRT1 were a kind gift from Erin Connolly (Connolly et al., 2002), and antibodies against ferritin were kindly provided by Frédéric Gaymard (Dellagi et al., 2005). The monoclonal antibody against *Arabidopsis* actin (MA1-744) was from Affinity BioReagents; antisera against Atm1 and Nfs1 were described previously (Kispal et al., 1999).

### Dual-PAM Analysis

Chlorophyll fluorescence parameters and the redox change of P700 were assessed with a Dual-PAM-100 measuring system (Walz) in 4-week-old plants. The maximum PSII quantum yield,  $F_v/F_m$ , was measured in dark-adapted plants with  $F_v/F_m = (F_m - F_o)/F_m$ .

P700 oxidation was monitored by absorbance changes at 820 nm ( $\Delta A_{820}$ ) relative to an  $A_{820}$  calibration ( $\Delta A_{820}/A_{820}$ ). The maximal  $\Delta A_{820}$  (Pm; P700 fully oxidized) was determined by application of a saturation pulse after 10 s of far-red preillumination. Y(NA), the quantum yield of nonphotochemical energy dissipation due to acceptor-side limitation, was calculated based on a Pm' determination at  $220 \mu\text{mol m}^{-2} \text{s}^{-1}$  actinic light according to:  $Y(NA) = (Pm - Pm')/Pm$ .

### Miscellaneous Methods

Chlorophyll extraction in 80% (v/v) acetone (Lichtenthaler, 1987), Alexander's stain for pollen viability (Johnson-Brousseau and McCormick, 2004), quantification of total iron using the iron chelator ferene (Hennessy et al., 1984) or inductively coupled plasma-mass spectrometry, as indicated;

root length measurements and densitometry were carried out with ImageJ software.

## Supplemental Data

The following materials are available in the online version of this article.

**Supplemental Figure S1.** Plastid chlorophyll levels and chloroplast counts in *atm3-1*.

**Supplemental Figure S2.** Quantification of ACO1 in-gel activity.

**Supplemental Figure S3.** PSI activity in isolated chloroplasts in *atm3-1*.

**Supplemental Figure S4.** Sequence alignment of Arabidopsis ATM1, ATM2, and ATM3 and related proteins.

**Supplemental Table S1.** List of primers.

## ACKNOWLEDGMENTS

We thank Susie Vernon, Louise Fets, Charlotte Leese, Allan Jones, Edward Hagues, Sarah Shiales, and Emma Smiles for help with the project; Roland Lill and Sabine Molnik (Philipps University Marburg) for raising Arabidopsis aconitase antibodies; Erin Connolly (University of South Carolina) for antibodies against IRT1; Frédéric Gaymard and Jean-François Briat (University of Montpellier) for antibodies against AtFer1; Dario Leister (University of Munich) for *irt1-1* seeds; Steve McGrath (Rothamsted Research) for element analysis; Sergei Kushnir (University of Ghent) for the *sta1* mutant line and general discussion; and Julia Teschner, Florian Bittner, and Ralf Mendel (TU Braunschweig) for mutant lines and discussion.

Received June 25, 2009; accepted August 20, 2009; published August 26, 2009.

## LITERATURE CITED

- Arnaud N, Ravet K, Borlotti A, Touraine B, Boucherez J, Fizames C, Briat JF, Cellier F, Gaymard F (2007) The iron-responsive element (IRE)/iron-regulatory protein 1 (IRP1)-cytosolic aconitase iron-regulatory switch does not operate in plants. *Biochem J* **405**: 523–531
- Aronsson H, Jarvis P (2002) A simple method for isolating import-competent *Arabidopsis* chloroplasts. *FEBS Lett* **529**: 215–220
- Babiychuk E, Fuangthong M, Van Montagu M, Inzé D, Kushnir S (1997) Efficient gene tagging in *Arabidopsis thaliana* using a gene trap approach. *Proc Natl Acad Sci USA* **94**: 12722–12727
- Balk J, Lobréaux S (2005) Biogenesis of iron-sulfur proteins in plants. *Trends Plant Sci* **10**: 324–331
- Brugière S, Kowalski S, Ferro M, Seigneurin-Berny D, Miras S, Salvi D, Ravanel S, d'Hérin P, Garin J, Bourguignon J, et al (2004) The hydrophobic proteome of mitochondrial membranes from *Arabidopsis* cell suspensions. *Phytochemistry* **65**: 1693–1707
- Bych K, Netz DJ, Viganì G, Bill E, Lill R, Pierik AJ, Balk J (2008) The essential cytosolic iron-sulfur protein Nbp35 acts without Cfd1 partner in the green lineage. *J Biol Chem* **283**: 35797–35804
- Cavazza C, Martin L, Mondy S, Gaillard J, Ratet P, Fontecilla-Camps JC (2008) The possible role of an [FeFe]-hydrogenase-like protein in the plant responses to changing atmospheric oxygen levels. *J Inorg Biochem* **102**: 1359–1365
- Chen S, Sánchez-Fernández R, Lyver ER, Dancis A, Rea PA (2007) Functional characterization of AtATM1, AtATM2, and AtATM3, a subfamily of *Arabidopsis* half-molecule ATP-binding cassette transporters implicated in iron homeostasis. *J Biol Chem* **282**: 21561–21571
- Connolly EL, Fett JP, Gueriot ML (2002) Expression of the IRT1 metal transporter is controlled by metals at the levels of transcription and protein accumulation. *Plant Cell* **14**: 1347–1357
- Curie C, Briat JF (2003) Iron transport and signaling in plants. *Annu Rev Plant Biol* **54**: 183–206
- Dai X, Hayashi K, Nozaki H, Cheng Y, Zhao Y (2005) Genetic and chemical analysis of the action mechanisms of sirtinol in *Arabidopsis*. *Proc Natl Acad Sci USA* **102**: 3129–3134
- Daum G, Gasser SM, Schatz G (1982) Import of proteins into mitochondria: energy-dependent, two-step processing of the intermembrane space enzyme cytochrome *b*<sub>2</sub> by isolated yeast mitochondria. *J Biol Chem* **257**: 13075–13080
- Dawson RJP, Locher KP (2006) Structure of a bacterial multidrug ABC transporter. *Nature* **443**: 180–185
- Day DA, Neuburger M, Douce R (1985) Biochemical characterization of chlorophyll-free mitochondria from pea leaves. *Aust J Plant Physiol* **12**: 219–228
- Dellagi A, Rigault M, Segond D, Roux C, Kraepiel Y, Cellier F, Briat J-F, Gaymard F, Expert D (2005) Siderophore-mediated upregulation of Arabidopsis ferritin expression in response to *Erwinia chrysanthemi* infection. *Plant J* **43**: 262–272
- Eastmond PJ, Germain V, Lange PR, Bryce PR, Smith SM, Graham IA (2000) Postgerminative growth and lipid catabolism in oilseeds lacking the glyoxylate cycle. *Proc Natl Acad Sci USA* **97**: 5669–5674
- Ferro M, Salvi D, Brugière S, Miras S, Kowalski S, Louwagie M, Garin J, Joyard J, Rolland N (2003) Proteomics of the chloroplast envelope membranes from *Arabidopsis thaliana*. *Mol Cell Proteomics* **2**: 325–345
- Frazzon AP, Ramirez MV, Warek U, Balk J, Frazzon J, Dean DR, Winkel BS (2007) Functional analysis of Arabidopsis genes involved in mitochondrial iron-sulfur cluster assembly. *Plant Mol Biol* **64**: 225–240
- Froehlich JE, Wilkerson CG, Ray WK, McAndrew RS, Osteryoung KW, Gage DA, Phinney BS (2003) Proteomic study of the *Arabidopsis thaliana* chloroplast envelope membrane utilizing alternatives to traditional two-dimensional electrophoresis. *J Proteome Res* **2**: 413–425
- Heazlewood JL, Tonti-Filippini JS, Gout AM, Day DA, Whelan J, Millar AH (2004) Experimental analysis of the *Arabidopsis* mitochondrial proteome highlights signaling and regulatory components, provides assessment of targeting prediction programs, and indicates plant-specific mitochondrial proteins. *Plant Cell* **16**: 241–256
- Hennessy DJ, Reid GR, Smith FE, Thompson SL (1984) Ferene: a new spectrophotometric reagent for iron. *Can J Chem* **62**: 721–724
- Imssande J (1999) Iron-sulfur clusters: formation, perturbation, and physiological functions. *Plant Physiol Biochem* **37**: 87–97
- Johnson-Brousseau SA, McCormick S (2004) A compendium of methods useful for characterizing Arabidopsis pollen mutants and gametophytically-expressed genes. *Plant J* **39**: 761–775
- Kessler D (2006) Enzymatic activation of sulfur for incorporation into biomolecules in prokaryotes. *FEMS Microbiol Rev* **30**: 825–840
- Kessler D, Papenbrock J (2005) Iron-sulfur cluster biosynthesis in photosynthetic organisms. *Photosynth Res* **86**: 391–407
- Kim DY, Bovet L, Kushnir S, Noh EW, Martinoia E, Lee Y (2006) AtATM3 is involved in heavy metal resistance in Arabidopsis. *Plant Physiol* **140**: 922–932
- Kim DY, Bovet L, Maeshima M, Martinoia E, Lee Y (2007) The ABC transporter AtPDR8 is a cadmium extrusion pump conferring heavy metal resistance. *Plant J* **50**: 207–218
- Kispal G, Csere P, Guiard B, Lill R (1997) The ABC transporter Atm1p is required for mitochondrial iron homeostasis. *FEBS Lett* **418**: 346–350
- Kispal G, Csere P, Prohl C, Lill R (1999) The mitochondrial proteins Atm1p and Nfs1p are essential for biogenesis of cytosolic Fe/S proteins. *EMBO J* **18**: 3981–3989
- Kohbushi H, Nakai Y, Kikuchi S, Yabe T, Hori H, Nakai M (2009) Arabidopsis cytosolic Nbp35 homodimer can assemble both [2Fe-2S] and [4Fe-4S] clusters in two distinct domains. *Biochem Biophys Res Commun* **378**: 810–815
- Koshiba T, Saito E, Ono N, Yamamoto N, Sato M (1996) Purification and properties of flavin- and molybdenum-containing aldehyde oxidase from coleoptiles of maize. *Plant Physiol* **110**: 781–789
- Kuhnke G, Neumann K, Mühlhoff U, Lill R (2006) Stimulation of the ATPase activity of the yeast mitochondrial ABC transporter Atm1p by thiol compounds. *Mol Membr Biol* **23**: 173–184
- Kushnir S, Babiychuk E, Storozhenko S, Davey MW, Papenbrock J, De Rycke R, Engler G, Stephan UW, Lange H, Kispal G, et al (2001) A mutation of the mitochondrial ABC transporter Sta1 leads to dwarfism and chlorosis in the *Arabidopsis* mutant *starik*. *Plant Cell* **13**: 89–100
- Leighton J, Schatz G (1995) An ABC transporter in the mitochondrial inner membrane is required for normal growth of yeast. *EMBO J* **14**: 188–195
- Lichtenthaler HK (1987) Chlorophylls and carotenoids: pigments of photosynthetic biomembranes. *Methods Enzymol* **148**: 350–382
- Lill R, Mühlhoff U (2008) Maturation of iron-sulfur proteins in eukaryotes: mechanisms, connected processes, and diseases. *Annu Rev Biochem* **77**: 669–700
- Mendel RR, Bittner F (2006) Cell biology of molybdenum. *Biochim Biophys Acta* **1763**: 621–635

- Mikolay A, Nies DH** (2009) The ABC-transporter AtmA is involved in nickel and cobalt resistance in *Cupriavidus metallidurans* strain CH34. *Antonie van Leeuwenhoek* **96**: 183–191
- Moeder W, del Pozo O, Navarre D, Martin GB, Klessig DF** (2007) Aconitase plays a role in regulating resistance to oxidative stress and cell death in *Arabidopsis* and *Nicotiana benthamiana*. *Plant Mol Biol* **63**: 273–287
- Pilon M, Abdel-Ghany SE, Van Hoewyk D, Ye H, Pilon-Smits EA** (2006) Biogenesis of iron-sulfur cluster proteins in plastids. *Genet Eng (NY)* **27**: 101–117
- Pondarré C, Antiochos BB, Clarke SL, Greer EL, Deck KM, McDonald A, Han AP, Medlock A, Kutok JL, Anderson SA, et al** (2006) The mitochondrial ATP-binding cassette transporter Abcb7 is essential in mice and participates in cytosolic iron-sulfur cluster biogenesis. *Hum Mol Genet* **15**: 953–964
- Prime TA, Sherrier DJ, Mahon P, Packman LC, Dupree P** (2000) A proteomic analysis of organelles from *Arabidopsis thaliana*. *Electrophoresis* **21**: 3488–3499
- Rea PA** (2007) Plant ATP-binding cassette transporters. *Annu Rev Plant Biol* **58**: 347–375
- Rouault TA, Tong WH** (2008) Iron-sulfur cluster biogenesis and human disease. *Trends Genet* **24**: 398–407
- Rutherford JC, Ojeda L, Balk J, Mühlhoff U, Lill R, Winge DR** (2005) Activation of the iron regulon by the yeast Aft1/Aft2 transcription factors depends on mitochondrial but not cytosolic iron-sulfur protein biogenesis. *J Biol Chem* **280**: 10135–10140
- Schiestl RH, Gietz RD** (1989) High efficiency transformation of intact yeast cells using single stranded nucleic acids as a carrier. *Curr Genet* **16**: 339–346
- Somerville CR, Ogren WL** (1981) Photorespiration-deficient mutants of *Arabidopsis thaliana* lacking mitochondrial serine transhydroxymethylase activity. *Plant Physiol* **67**: 666–671
- Stehling O, Smith PM, Biederbick A, Balk J, Lill R, Mühlhoff U** (2007) Investigation of iron-sulfur protein maturation in eukaryotes. *Methods Mol Biol* **372**: 325–342
- Sweetlove LJ, Taylor NL, Leaver CJ** (2007) Isolation of intact, functional mitochondria from the model plant *Arabidopsis thaliana*. *Methods Mol Biol* **372**: 125–136
- Takahashi M, Sasaki Y, Ida S, Morikawa H** (2001) Nitrite reductase gene enrichment improves assimilation of NO<sub>2</sub> in *Arabidopsis*. *Plant Physiol* **126**: 731–741
- Touraine B, Boutin JP, Marion-Poll A, Briat JF, Peltier G, Lobréaux S** (2004) Nfu2: a scaffold protein required for [4Fe-4S] and ferredoxin iron-sulfur cluster assembly in *Arabidopsis* chloroplasts. *Plant J* **40**: 101–111
- Van Hoewyk D, Abdel-Ghany SE, Cohu CM, Herbert SK, Kugrens P, Pilon M, Pilon-Smits EA** (2007) Chloroplast iron-sulfur cluster protein maturation requires the essential cysteine desulfurase CpNifS. *Proc Natl Acad Sci USA* **104**: 5686–5691
- Varotto C, Maiwald D, Pesaresi P, Jahns P, Salamini F, Leister D** (2002) The metal ion transporter IRT1 is necessary for iron homeostasis and efficient photosynthesis in *Arabidopsis thaliana*. *Plant J* **31**: 589–599
- Verrier PJ, Bird D, Burla B, Dassa E, Forestier C, Geisler M, Klein M, Kolukisaoglu Ü, Lee Y, Martinoia E, et al** (2008) Plant ABC proteins: a unified nomenclature and updated inventory. *Trends Plant Sci* **13**: 151–159
- Xu XM, Möller SG** (2008) Iron-sulfur cluster biogenesis systems and their crosstalk. *ChemBioChem* **9**: 2355–2362
- Yabe T, Morimoto K, Kikuchi S, Nishio K, Terashima I, Nakai M** (2004) The *Arabidopsis* chloroplastic NifU-like protein CnfU, which can act as an iron-sulfur cluster scaffold protein, is required for biogenesis of ferredoxin and photosystem I. *Plant Cell* **16**: 993–1007
- Zhao Y, Dai X, Blackwell HE, Schreiber SL, Chory J** (2003) SIR1, an upstream component in auxin signaling identified by chemical genetics. *Science* **301**: 1107–1110
- Zybailov B, Rutschow H, Friso G, Rudella A, Emanuelsson O, Sun Q, van Wijk KJ** (2008) Sorting signals, N-terminal modifications and abundance of the chloroplast proteome. *PLoS One* **3**: e1994

# CORRECTIONS

## Vol. 151: 590–602, 2009

Bernard D.G., Cheng Y., Zhao Y., and Balk J. An Allelic Mutant Series of *ATM3* Reveals Its Key Role in the Biogenesis of Cytosolic Iron-Sulfur Proteins in Arabidopsis.

The ACO3 protein and the *aco3* mutant in this article correspond to, respectively, the ACO2 (AT4G26970) protein and the *aco2-1* mutant in Arnaud et al. (2007). ACO2 and *aco2* in this article correspond to ACO3 (AT2G05710) in Arnaud et al. (2007) and KO-661 in Moeder et al. (2007). The link between the mutant symbols and the stock center codes in this article can be found in the “Materials and Methods” and is correct. Since ACO2 and ACO3 are both localized in mitochondria, and have normal enzyme activities in *atm3* mutants, in contrast to the cytosolic ACO1, the interchanged nomenclature does not affect the conclusions of the article. We apologize for any confusion and we fully support the nomenclature of Arnaud et al. (2007).

---

[www.plantphysiol.org/cgi/doi/10.1104/pp.109.900309](http://www.plantphysiol.org/cgi/doi/10.1104/pp.109.900309)

## Vol. 151: 603–619, 2009

Meyer E.H., Tomaz T., Carroll A.J., Estavillo G., Delannoy E., Tanz S.K., Small I.D., Pogson B.J., and Millar A.H. Remodeled Respiration in *ndufs4* with Low Phosphorylation Efficiency Suppresses Arabidopsis Germination and Growth and Alters Control of Metabolism at Night.

A corruption and error in microarray data analysis resulted in incorrect reports of the fold changes in differentially expressed genes identified in both *ndufs4* and *ndufa1* mutants reported in Supplemental Data S1 and Supplemental Tables S2 to S4. Corrected versions of these supplemental files have now been provided. These differences do not affect statements in the abstract, or any of the data displays in the article itself, or the major conclusions of the study.

However, while all the genes and gene sets in functional bins noted in the text of this article are still significantly different in the mutants, a number of statements about the direction of these microarray changes in the “Results” and “Discussion” text are incorrect. In references to Supplemental Table S2, processes involving protein metabolism (BIN 29), the cell cycle (BIN 31.3), RNA metabolism (BIN 27.1, BIN 27.4), development (BIN 33), and mitochondrial electron transport (BIN 9) were significantly up-regulated (not down-regulated) in the mutants, while photosynthetic (BIN 1), light-signaling (BIN 30.11), and stress (BIN 20) genes were significantly down-regulated (not up-regulated) in the mutants. In reference to Supplemental Table S3, amongst the external NADH dehydrogenase transcripts, NDA1 was the only one decreased (not increased) in *ndufs4* and *ndufa1*, which is now consistent with the protein level changes noted in Figure 3G.

The suggestion made in the article that the data differ from the transcriptional decrease in photosynthetic light reaction gene expression observed in response to rotenone inhibition (Garmier et al., 2008) is incorrect. The transcriptional changes in photosynthetic genes in *ndufs4* and *ndufa1* are in the same general direction as in that study.

**Garmier M, Carroll AJ, Delannoy E, Vallet C, Day DA, Small ID, Millar AH (2008) Complex I dysfunction redirects cellular and mitochondrial metabolism in Arabidopsis. *Plant Physiol* 148: 1324–1341**

---

[www.plantphysiol.org/cgi/doi/10.1104/pp.109.900310](http://www.plantphysiol.org/cgi/doi/10.1104/pp.109.900310)